

Kinetics and thermodynamics of proton transfer to Cp^{*}Ru(dppe)H: Via dihydrogen bonding and (η²-H₂)-complex to the dihydride

Natalia V. Belkova ^{a,*}, Pavel A. Dub ^a, Miguel Baya ^{b,c}, Jennifer Houghton ^b

^a Nesmeyanov Institute of Organoelement Compounds, Russian Academy of Sciences, Vavilov Street 28, 119991 Moscow, Russia

^b Laboratoire de Chimie de Coordination, UPR CNRS 8241 liée par convention à l'Université Paul Sabatier et à l'Institut National Polytechnique de Toulouse, 205 Route de Narbonne, 31077 Toulouse Cedex, France

^c Departament de Química, Edifici C.n, Universitat Autònoma de Barcelona, 08193 Bellaterra, Catalonia, Spain

Received 16 June 2006; received in revised form 31 July 2006; accepted 31 July 2006

Available online 18 August 2006

Inorganic Chemistry – The Next Generation.

Abstract

The interaction between Cp^{*}RuH(dppe) and a series of proton donors (HA) of increasing strength: CFH₂CH₂OH (MFE), CF₃CH₂OH (TFE), (CF₃)₂CHOH (HFIP), *p*-nitrophenol, CF₃COOH and HBF₄ has been investigated spectroscopically by variable-temperature IR, UV–Vis, and NMR spectroscopy in solvents of differing polarity (*n*-hexane, dichloromethane and their mixture). The low-temperature IR study shows the establishment of a hydrogen-bond which involves the hydride ligand as the proton accepting site. The basicity factor E_j for the hydride was found to be 1.39. All techniques indicate that an equilibrium exists between the dihydrogen-bonded complex and the cationic dihydrogen complex, [Cp^{*}Ru(η²-H₂)(dppe)]⁺, the formation of which is shown here for the first time. The proton transfer from HFIP is characterized by $\Delta H^\ddagger = -8.1 \pm 0.6$ kcal mol⁻¹ and $\Delta S^\ddagger = -17 \pm 3$ eu. The activation parameters for the subsequent irreversible isomerization leading to the classical dihydride complex, [Cp^{*}Ru(H)₂(dppe)]⁺, are $\Delta H^\ddagger = 20.9 \pm 0.8$ kcal mol⁻¹ and $\Delta S^\ddagger = 9 \pm 3$ eu as determined from ¹H NMR spectroscopy for protonation by HBF₄. Computational results at the DFT/B3PW91 level confirm the experimentally observed hydride basicity increase on descending the Group from iron to ruthenium and also the formation of the non-classical complex as an intermediate, prior to the thermodynamically favored dihydride.
© 2006 Elsevier B.V. All rights reserved.

Keywords: Dihydrogen bonding; Proton transfer; Hydride complexes; Ruthenium; DFT calculations

1. Introduction

Proton-transfer processes to and from transition metal hydride complexes are the key steps in many stoichiometric and catalytic chemical and biochemical processes [1]. It is nowadays well established that the interaction with the hydride ligand leads to a dihydrogen complex via dihydrogen bonded (MH···HA) adduct, whereas interaction with the metal atom affords a M···HA hydrogen bond and then a polyhydride species [2]. Dihydrogen complexes are sometimes unstable (therefore they are often

called “kinetic protonation products”) and further evolve to thermodynamically favored products – classical polyhydrides [3]. From general considerations, the preponderance of either reaction pathway will be determined by a combination of both the nature of the metal center and the electronic and steric properties of the ligands in its coordination sphere. However, the current knowledge is far from allowing to predict the reaction mechanism in any given case. In particular, a change of central metal atom down a Group may lead not only to an increase of hydride ligand basicity and strengthening of dihydrogen bonded complexes [4], but also to a change of proton accepting site and to a direct interaction with the metal (M···HA hydrogen bonding). As an illustrative example,

* Corresponding author. Tel.: +7 495 1356448; fax: +7 495 1355085.
E-mail address: nataliabelk@ineos.ac.ru (N.V. Belkova).

hydrogen bond to the hydride ligand precedes the proton transfer to $\text{Cp}^*\text{MoH}_3(\text{dppe})$ ($\text{Cp}^* = (\eta^5\text{-C}_5\text{Me}_5)$, $\text{dppe} = 1,2\text{-bis}(\text{diphenylphosphino})\text{ethane}$) [5], whereas the formation of an hydrogen bond to the metal atom is the first step in protonation of tungsten analogue $\text{Cp}^*\text{WH}_3(\text{dppe})$ [5a], the reaction product being classical tetrahydride $[\text{Cp}^*\text{MH}_4(\text{dppe})]^+$ in both cases.

Our previous works on the $\text{Cp}^*\text{FeH}(\text{dppe})$ species [6,7] have proved that, for this complex, the nucleophilic center is the hydride site. The strength and concentration of the proton donor determine the evolution of the dihydrogen-bonded adduct to a dihydrogen species, which can further evolve to the classical dihydride complex in an irreversible process. We have found that the strength of the dihydrogen-bonding interaction correlates with the proton transfer barrier. In the case of rather weak proton donors (like fluorinated alcohols), the presence of a second molecule of acid is required to trigger the proton transfer, through the enhancement of the primary dihydrogen bond strength and the stabilization of the transition state and of the final product by homoconjugated anion formation. The activation parameters of the dihydrogen to dihydride isomerization process in the reaction with strong acids (HBF_4 and TFA) have been determined, as well as the isotope effects derived from the hydride H/D isotopic substitution [8]. The theoretical analysis of the potential energy surfaces for the isomerization of the non-classical complex into the classical one and comparison of theoretical and experimental isotope effects have led to the final elucidation of the mechanism (Scheme 1).

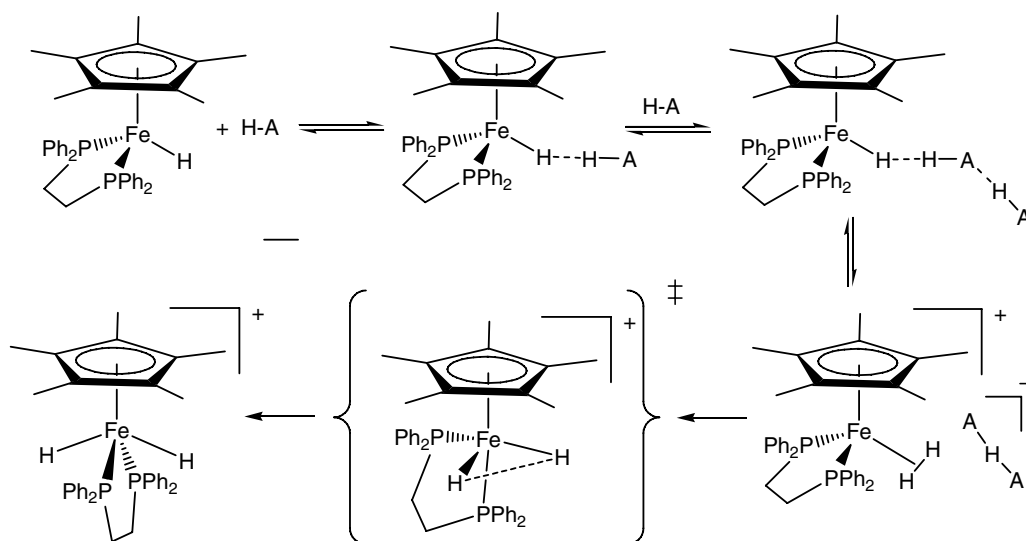
The ruthenium analogue of the above iron hydride, $\text{Cp}^*\text{RuH}(\text{dppe})$, is known [9] and has been recently tested together with other ruthenium hydride complexes $\text{Cp}'\text{RuH}(\text{PP})$ ($\text{Cp}' = \text{C}_5\text{H}_5, \text{C}_5\text{H}_4\text{Me}, \text{C}_5\text{Me}_5$; $\text{PP} = \text{chelating diposphine}$) as an iminium cation hydrogenation catalyst [10]. Although the $\text{Cp}^*\text{RuH}(\text{dppe})$ protonation has

not been studied, the cationic $[\text{Cp}^*\text{RuH}_2(\text{dppe})]^+$ complex, obtained by H_2 addition to $[\text{Cp}^*\text{Ru}(\text{dppe})]^+$, is known to be a *trans*-dihydride [11]. Therefore, one cannot exclude a priori the direct attack of a proton donor on the metal atom and formation of $\text{Ru} \cdots \text{HA}$ hydrogen bond as the incipient step of proton transfer in this case. Thus, in order to further study the problem of metal influence on the nature and properties of hydrogen bonded intermediates along the proton transfer pathway to transition metal hydride complexes, we have extended our investigations to the ruthenium species $\text{Cp}^*\text{RuH}(\text{dppe})$.

In this paper, we report the results of combined variable temperature (190–290 K) spectroscopic and theoretical studies of the interaction between $\text{Cp}^*\text{RuH}(\text{dppe})$ and proton donors (HA) of increasing acid strength: $\text{CFH}_2\text{CH}_2\text{OH}$ (MFE), $\text{CF}_3\text{CH}_2\text{OH}$ (TFE), $(\text{CF}_3)_2\text{CHOH}$ (HFIP), *p*-nitrophenol, CF_3COOH and HBF_4 in solvents of different polarities (*n*-hexane, dichloromethane and their mixture). We have undertaken the equilibrium thermodynamics investigation of the proton transfer step for the system $[\text{Cp}^*\text{Ru}(\text{dppe})\text{H}]/\text{HFIP}$ and a variable temperature kinetic study of the subsequent process of the *trans*- $[\text{Cp}^*\text{Ru}(\text{H})_2(\text{dppe})]^+$ dihydride formation to gain information on the activation parameters of this step.

2. Experimental

All manipulations were performed under argon atmosphere by standard Schlenk techniques. All solvents were dried over appropriate drying agent (Na/benzophenone for benzene or THF, CaH_2 for dichloromethane, Na for *n*-hexane) and freshly distilled under an argon atmosphere prior to use. CD_2Cl_2 for NMR experiments (99.96 at.% D) by Aldrich was degassed by three freeze–pump–thaw cycles, and then purified by vacuum transfer at room temperature. All $\text{Cp}^*\text{Ru}(\text{dppe})\text{H}$ -solutions in CH_2Cl_2 were



Scheme 1.

prepared and kept up at 190–200 K (iso-propanol/liquid N₂ baths) due to low stability of Cp^{*}Ru(dppe)H in CH₂Cl₂ at room temperature (see below).

2.1. Preparation of Cp^{*}Ru(dppe)H

Metallic sodium (150 mg, 6.4 mmol) was added over dry methanol (60 mL). When the reaction was completed, a toluene solution (30 mL) of Cp^{*}RuCl(dppe) (1.24 g, 1.85 mmol) [12] was added and the mixture was heated to reflux for 5 h. The solvent was removed in vacuo, the residue was extracted with toluene (20 mL) and filtered through celite. The obtained solution was vacuum-dried and the residue was washed with cold methanol (10 mL, –40 °C). The resulting solid was vacuum-dried and recrystallized from *n*-hexane. A light-yellow powder was obtained. Yield: 0.85 g (72%).

¹H NMR (250 MHz, C₆D₆): δ –13.43 (t, ²J_{H–P} = 35 Hz, 1H, Ru–H), 1.84 (s, 15H, Cp^{*}), 2.09–1.84 (m, 4 H, –CH₂–CH₂–), 7.10–8.00 (m, 20H, Ph); T_{1min} = 787 ms at 233 K in CD₂Cl₂. ³¹P{¹H} NMR (101 MHz, C₆D₆): δ 90.2 (s). IR (nujol, CaF₂): 1900 cm^{–1} (ν_{RuH}).

2.2. Spectroscopic studies

2.2.1. IR and UV–Vis investigations

The IR measurements were performed on the “Infracum 801” FT-IR and “Specord M82” spectrometers using CaF₂ cells of 0.04–0.12 cm path length. UV measurements were performed on “Specord M-40” spectrometer. All IR and UV measurements were carried out by use of a home-modified cryostat (Carl Zeiss Jena) in the 190–290 K temperature range. The cryostat modification allows operating under an inert atmosphere and transferring the reagents (premixed either at low or room temperature) directly into the cell which is pre-cooled to the required temperature. The accuracy of the temperature adjustment was ±1 K. This setup was used both for the variable-temperature equilibrium studies and for the kinetics investigations at different temperatures.

2.2.2. NMR investigations

Samples of the hydride **1** in CD₂Cl₂ were prepared under an argon atmosphere in 5 mm NMR tubes and cooled down to 195 K immediately after dissolving. 58% HBF₄ · Et₂O or TFE was added to the pre-cooled solution just before the measurements.

The ¹H and ³¹P{¹H} data were collected with a Bruker AV500 spectrometer operating at 500.3 and 202.5 MHz, respectively. The temperature was calibrated using a methanol chemical shift thermometer; the accuracy and stability was ±1 K. All samples were allowed to equilibrate at every temperature for at least 3–5 min. The spectra were calibrated with the residual solvent resonance (¹H) and with external 85% H₃PO₄ (³¹P). The conventional inversion-recovery method (180–τ–90) was used to determine the variable-temperature longitudinal relaxation time T₁.

Standard Bruker software was used for the calculation of the longitudinal relaxation time.

2.3. Electrochemical measurements

Cyclic voltammograms were recorded with an EG&G 362 potentiostat connected to a Macintosh computer through MacLab hardware/software. The electrochemical cell was fitted with an Ag/AgCl reference electrode, a 1 mm diameter Pd-disk working electrode, and a platinum-wire counter electrode. [Bu₄N]PF₆ (ca. 0.1 M) was used as the supporting electrolyte. All potentials are reported relative to the ferrocene/ferrocenium couple. Ferrocene was added and measured as an internal standard at the end of the experiment.

2.4. Computational details

Quantum mechanical calculations were performed with the GAUSSIAN 03 package [13] at the DFT B3PW91 level [14]. The phenyl groups of the dppe ligand were substituted by hydrogens in the model complexes. Core electrons of the Ru and P atoms were described using the effective core pseudopotentials of Hay–Wadt [15] and valence electrons were described with the standard LANL2DZ basis set [13]. In the case of the P atoms, a set of d-type functions was added [16]. All carbon atoms, the hydrogen atoms not bonded to the metal, and the atoms of the TFE not involved in a hydrogen bond have been described with a 6-31G basis set [17]. The hydrogen atom directly bonded to the Ru center, together with hydrogen and oxygen atoms of the proton donors involved in the hydrogen bonding have been described with a 6-31G(d,p) basis set [17]. Minima and transition states were characterized by analytically computing the Hessian matrix. The basis set superposition errors were calculated according to the counterpoise method of Boys and Bernardi [18].

3. Results

3.1. Synthesis, spectroscopic and electrochemical study of Cp^{*}Ru(dppe)H

The synthesis of Cp^{*}RuH(dppe) (**1**) was originally described in [9] where NaBH₄ in EtOH was used to reduce Cp^{*}RuCl(dppe) (**2**) and had a reported yield of 41%. Thus we explored other synthetic possibilities in order to improve the yield. Reduction with LiAlH₄ in THF at room temperature for 2 h, the simplest method for preparing the iron analogue, does not work in the ruthenium case, but **1** is obtained after a 2 h reflux, although with a poor yield (42%). However, another well-known approach [19] – reduction with sodium methoxide in a methanol/toluene mixture – gave higher yields (up to 72%). The main spectroscopic features of **1** are a triplet at –13.43 ppm (²J_{HP} = 35 Hz) in the high field region of the ¹H NMR spectrum, and a singlet at 90.2 ppm in the ³¹P{¹H} NMR

spectrum, measured at room temperature in a benzene- d_6 solution. The position of the hydride resonance is solvent and temperature dependent, shifting from -14.11 to -14.20 ppm upon cooling the solution of **1** in dichloromethane from 253 to 193 K. In the IR spectrum (THF solution), it shows a ν_{RuH} band at 1916 cm^{-1} .

Complex **1** is very soluble in benzene, toluene and THF, and sparingly soluble in methanol. No significant H/D exchange was observed at the hydride site when stirring a suspension of **1** in methanol- d_4 for 4 days, as observed by ^1H , ^2H and $^{31}\text{P}\{^1\text{H}\}$ NMR spectroscopy. As many other hydride species, it is not stable in dichloromethane and evolves to the chloride derivative **2** by H/Cl exchange with the solvent. This is evidenced by the appearance of a quintuplet in the ^1H NMR spectrum at 3.04 ppm ($^2J_{\text{HD}} = 1.6\text{ Hz}$), assigned to CHD_2Cl , and a singlet in the $^{31}\text{P}\{^1\text{H}\}$ spectrum at 75.2 ppm, assigned to $\text{Cp}^*\text{RuCl}(\text{dppe})$, when following the evolution of **1** in CD_2Cl_2 . At 300 K, the transformation is of about 15% in 1 h, and almost quantitative ($>90\%$) after 24 h, the pseudo-first order rate constant for this reaction being $2.7 \times 10^{-5}\text{ s}^{-1}$ at 300 K. At lower temperatures ($<273\text{ K}$), **1** is perfectly stable in dichloromethane solutions allowing to run variable temperature protonation studies.

Cyclic voltammetric measurements of **1** in THF solution showed the presence of two oxidation processes at -0.38 and $+0.09\text{ V}$ relative to the ferrocene/ferrocenium (Fc) couple (Fig. 1). The first process is reversible and corresponds to the one electron oxidation of **1** to afford $[\text{Cp}^*\text{RuH}(\text{dppe})]^+$. The analogous $\text{Cp}^*\text{RuH}(\text{PR}_3)_2$ complexes [$(\text{PR}_3)_2 = (\text{PPh}_3)_2$, dppm , dppe , dppp] undergo one-electron oxidations at -0.1 to -0.3 V in THF or acetonitrile [20], whereas the related $(\eta^5\text{-C}_5\text{H}_4\text{R})\text{RuH}(\text{PPh}_3)_2$ complexes ($\text{R} = \text{H}$, $t\text{-Bu}$, CH_2Ph , CTol_3) yield $E_{1/2} = -0.36\text{ V}$ (independent of R) in dichloro-

methane [21]. Scanning to higher potentials allows a second oxidation process that is completely irreversible and causes partial loss in the reversibility of the first one. This suggests that the 2-electron oxidation product $[\text{Cp}^*\text{RuH}(\text{dppe})]^{2+}$ is immediately consumed by a chemical process, which also results in a concentration reduction for the 17-electron species formed in the first observed process. The same phenomenon was recently reported for the stepwise 2-electron oxidation of $\text{Cp}^*\text{MoH}_3(\text{dppe})$ [22] and attributed to the proton transfer from the 16-electron product of double oxidation to the starting material. For the oxidation of **1**, this corresponds to the process shown in Scheme 2 ($\text{S} = \text{solvent}$). The proton transfer process leads to the consumption of one equivalent of $\text{Cp}^*\text{RuH}(\text{dppe})$ by a non-electrochemical process for every two equivalents of the compound within the diffusion layer, thus reducing the return wave of the first oxidation process approximately by a factor of two. It is well known that the acidity of transition metal hydride complexes drastically increases upon oxidation [23]. Indeed, the stoichiometric one-electron oxidation with ferrocenium yielded $[\text{Cp}^*\text{Ru}(\text{H})_2(\text{dppe})]^+$ as the only identified hydride species.

3.2. Protonation by strong acids: characterization of $[\text{Cp}^*\text{Ru}(\text{dppe})\text{H}_2]^+$

Complex $[\text{Cp}^*\text{RuH}_2(\text{dppe})]^+$ is known [11] to have classical nature while other members of the $[\text{Cp}^*\text{RuH}_2(\text{PP})]^+$ family (where PP is bidentate phosphine or 2PPh_3) are non-classical ($\eta^2\text{-H}_2$) complexes at low temperatures and isomerize into $\text{trans-}[\text{Cp}^*\text{Ru}(\text{H})_2(\text{PP})]^+$ upon warming [24]. The existence of the non-classical form was not excluded [25], but was never confirmed.

Indeed, protonation of a dichloromethane- d_2 solution of **1** at 273 K and above with 1 or 2 equiv. HBF_4 immediately affords the classical dihydride $[\text{Cp}^*\text{Ru}(\text{H})_2(\text{dppe})]\text{BF}_4$ (**3**), which is stable in dichloromethane for several days. No visible traces of any other species were observed. The two main spectroscopic features of **3** are a triplet in the high field region of the ^1H NMR spectrum (-8.67 ppm , $^2J_{\text{H-P}} = 27.5\text{ Hz}$), and a singlet in the $^{31}\text{P}\{^1\text{H}\}$ NMR spectrum located at 71.3 ppm. However, when addition of acid was carried out at 193 K and the sample immediately monitored by low temperature NMR (193 K), quantitative formation ($>96\%$) of the non-classical $[\text{Cp}^*\text{Ru}(\eta^2\text{-H}_2)(\text{dppe})]^+\text{BF}_4^-$ (**4**) species was observed. A broad signal (half-height width $w_{1/2} = 60\text{ Hz}$) appeared at this temperature in the hydride region of the ^1H NMR spectrum, centered at -9.50 ppm in CD_2Cl_2 . Its $^{31}\text{P}\{^1\text{H}\}$ NMR spectrum shows a singlet at 77.4 ppm. Warming above 243 K led to the irreversible isomerization to the dihydride **3**. The important spectroscopic data for **1**, **3**, and **4** are shown in Table 1.

Longitudinal relaxation times of the hydride signals have been measured for the complexes **1**, **3** and **4** (Table 1). The

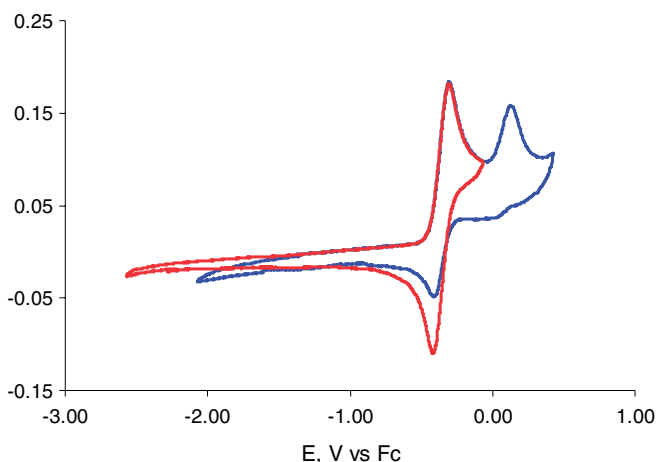
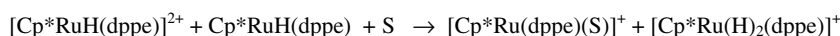


Fig. 1. Cyclic voltammograms for the oxidation of $\text{Cp}^*\text{RuH}(\text{dppe})$ in THF. Red trace: $-2.0\text{ V} / 0.5\text{ V}$. Blue trace: $-2.0\text{ V} / 1.0\text{ V}$. (Scan rate: 100 mV/s). (For interpretation of the references to color in this figure legend, the reader is referred to the web version of this article.)



Scheme 2.

Table 1

Selected IR, ^1H and $^{31}\text{P}\{^1\text{H}\}$ NMR spectroscopic characteristics for $\text{Cp}^*\text{Ru}(\text{dppe})\text{H}$ and $[\text{Cp}^*\text{Ru}(\text{dppe})\text{H}_2]^+\text{BF}_4^-$ in CD_2Cl_2

Compound	$\nu_{\text{Ru-H}}/\text{cm}^{-1}$ ($\epsilon/\text{M}^{-1}\text{cm}^{-1}$)	$\delta_{\text{H}}/\text{ppm}$ (J_{HP}/Hz)	$T_{1\text{min}}/\text{ms}$ (T/K)	δ_{P} (ppm)
$\text{Cp}^*\text{Ru}(\text{dppe})\text{H}$ (1)	1914 (255) ^a	-14.07 (32.5) ^b	787 (233)	89.3
$[\text{Cp}^*\text{Ru}(\text{dppe})(\text{H})_2]^+\text{BF}_4^-$ (3)	2000 (90) ^b	-8.67 (27.5) ^b	555 (213)	71.3 ^b
$[\text{Cp}^*\text{Ru}(\text{dppe})(\eta^2\text{-H}_2)]^+\text{BF}_4^-$ (4)	^c	-9.50 (broad) ^a	19.3 (233)	77.4 ^a

^a At 200 K.^b At 290 K.^c Not observable (see text).

T_1 minimum of **4** is found at about 233 K, and its value (19.3 ms) proves the non-classical nature of the product. Complex **3** shows a T_1 minimum of about 555 ms at 213 K, coherent with its dihydride formulation. The monohydride **1** shows a T_1 minimum of 787 ms at about 233 K.

Addition of ca. 1 equiv. of trifluoroacetic acid (TFA) to a CD_2Cl_2 solution of **1** at 193 K leads to the quantitative formation of the non-classical species **4**, as observed in the ^1H and $^{31}\text{P}\{^1\text{H}\}$ NMR spectra of this solution. An analogous procedure using CF_3COOD has allowed measuring the H–D coupling constant for the monolabelled dihydrogen ligand. No H/D scrambling has been H–D observed at this temperature, in the experimental timescale (approx. 30 min). The obtained value (23.8 Hz) corresponds to the H–D distance of 1.02 Å (calculated according to Eq. (1) [26]), which compares well with the value 1.07 Å obtained from the T_1 data assuming slow rotation of H_2 (Eq. (2) [27]).

$$r_{\text{HH}} = -0.0167 J_{\text{H-D}} + 1.42, \quad (1)$$

$$r_{\text{HH}} = 5.815(T_{1\text{min}}/\nu)^{1/6}. \quad (2)$$

In a parallel experiment carried out in CH_2Cl_2 , IR monitoring in the Ru–H stretching region provided the spectral changes shown in Fig. 2. The starting hydride complex **1** is characterized by a relatively strong asymmetric ν_{MH} band at 1914 cm^{-1} in CH_2Cl_2 solution, whose intensity grows up with lowering the temperature ($\epsilon = 255$ and $227\text{ L mol}^{-1}\text{ cm}^{-1}$ at 200 and 250 K, respectively). The asymmetry of the band is due to its overlap with the overtones of the aryl group vibrations and disappears after subtraction of the spectrum of $\text{Cp}^*\text{RuCl}(\text{dppe})$, see Fig. 2.

The HBF_4 addition at 200 K causes the complete disappearance of this band, see spectrum b. No new vibrations that could be unambiguously assigned to $\nu(\text{H-H})$ and $\nu(\text{M-H}_2)$ vibration modes for complex **4** appeared in the IR spectrum. These bands may be very weak or hidden under stronger CH vibrations or overtones. This spectrum remains essentially unchanged over time (over 40 min) at constant temperature, at temperatures below 230 K. At higher temperatures, slow conversion to the classical dihydride complex occurs, yielding eventually spectrum c. A new band at 2000 cm^{-1} is attributed to the cationic dihydride complex. Such significant high-frequency shift ($\Delta\nu = +86\text{ cm}^{-1}$) of the $\nu(\text{MH})$ band is typical for transition metal protonation yielding a cationic classical product [28].

Theoretical calculations have been carried out at the DFT B3PW91 level for the model $[\text{Cp}^*\text{RuH}_2(\text{dhpe})]^+$ com-

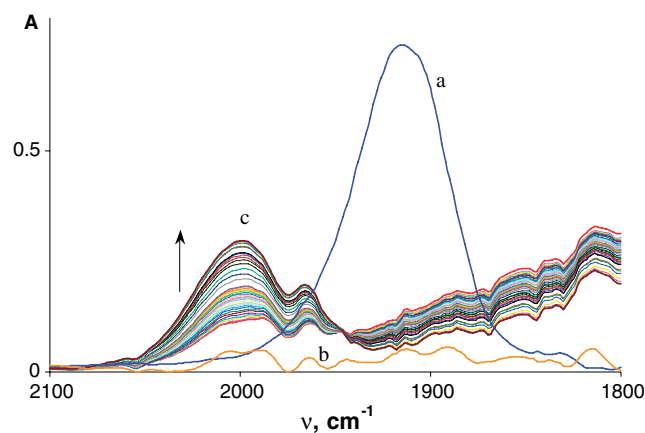


Fig. 2. IR spectra (ν_{RuH} region) of $\text{Cp}^*\text{RuH}(\text{dppe})$ (0.025 M) and $\text{Cp}^*\text{RuH}(\text{dppe})$ (0.025 M) in the presence of 1 equiv. HBF_4 in CH_2Cl_2 . Before the acid addition at 200 K (the spectrum of $\text{Cp}^*\text{RuCl}(\text{dppe})$ subtracted) (a); after addition of HBF_4 at 200 K (b) and 250 K, time-dependent spectra (c).

plex where the phenyl groups of the dppe ligand are substituted by hydrogens. Minima corresponding to the two expected isomers – dihydrogen complex and *trans*-dihydride – were revealed. The optimized geometries are presented in Fig. 3 and selected geometrical parameters are presented in Table 2. The energy difference between the dihydride and dihydrogen isomers of $[\text{Cp}^*\text{RuH}_2(\text{dhpe})]^+$ model complex is $2.25\text{ kcal mol}^{-1}$ in favor of the nonclassical isomer, which is less than that of the iron analogue ($4.90\text{ kcal mol}^{-1}$ [8]). Theoretical consideration of the different models for the $[\text{Cp}^*\text{FeH}_2(\text{PP})]^+$ (PP = dppe or dippe) [8] showed that the introduction of the substituents on the phosphine ligand enhances the stability of the dihy-

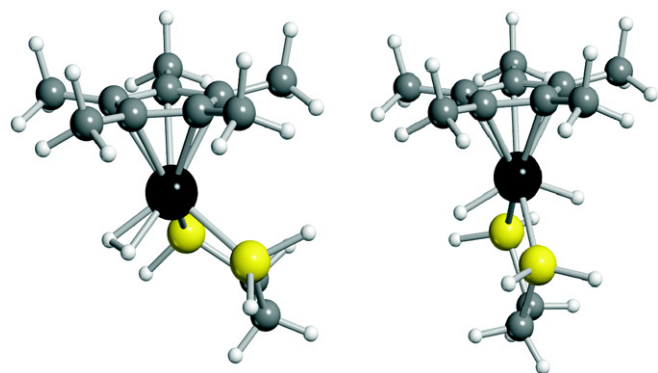


Fig. 3. Optimized geometries of the dihydrogen (left) and of the dihydride (right) isomers of the model complex $[\text{Cp}^*\text{RuH}_2(\text{dhpe})]^+$.

Table 2

Selected optimized geometrical parameters (bond lengths in Å and angles in °) of the dihydrogen and dihydride isomers of the model complex $[\text{Cp}^*\text{RuH}_2(\text{dhpe})]^+$

	$[\text{Ru}](\eta^2\text{-H}_2)^a$	$[\text{Ru}](\text{H})_2^a$
Ru–CNT ^b	1.92	1.92
Ru–P	2.32	2.31
Ru–H	2.32	2.30
H–H	1.71	1.62
	1.71	1.61
H–H	0.91	2.95
$\angle\text{P–Ru–P}$	82.4	87.0
$\angle\text{H–Ru–H}$	30.7	131.9

^a $[\text{Ru}]$: $[\text{Cp}^*\text{Ru}(\text{dhpe})]^+$.

^b CNT is the centroid of the Cp* ring.

dride form, reversing the stabilities in agreement with the experimental observations that the dihydride is the thermodynamic protonation product. Assuming a similar effect of the model for ruthenium, the calculations indicate that the relative stability of the dihydride isomer relative to the dihydrogen complex is greater for ruthenium.

3.3. Interaction with weak proton donors: characterization of hydrogen-bonded intermediate

To investigate the mechanism of the $\text{Cp}^*\text{RuH}(\text{dppe})$ protonation in more detail, we studied the interaction of **1** with fluorinated alcohols $\text{CFH}_2\text{CH}_2\text{OH}$ (MFE) and $(\text{CF}_3)_n\text{CH}_{3-n}\text{OH}$ (with $n = 1$ (TFE), 2 (HFIP)) according to the well-established protocol [29], using combination of IR and NMR spectroscopies. In the presence of excess hydride, the IR spectra in the ν_{OH} region show a typical picture of hydrogen bond formation. The intensity decrease of the alcohol (MFE and TFE) $\nu_{\text{OH}(\text{free})}$ bands is accompanied by the appearance of new broad low fre-

quency $\nu_{\text{OH}(\text{bonded})}$ bands of hydrogen bonded OH groups (Table 3). As expected, the interaction with the more fluorinated alcohol–TFE is stronger than with MFE, as indicated by the greater band shift $\Delta\nu_{\text{OH}} = \nu_{\text{OH}(\text{free})} - \nu_{\text{OH}(\text{bonded})}$. The interaction enthalpies were obtained using Iogansen's empirical correlation (Eq. (3)) [30,31] and from the temperature dependence of H-bond formation constants (van't Hoff method) (Table 3). Note that the H-bond formation entropies ΔS° are quite high in this case, which explains the low formation constants K , e.g. for the system **1**/TFE in dichloromethane $K_{200\text{K}}$ is only 10.4 M^{-1}

$$\Delta H^\circ = \frac{18\Delta\nu}{\Delta\nu + 720}, \quad (3)$$

$$E_j = \Delta H_{ij} / \Delta H_{11} P_i. \quad (4)$$

The combined study of IR changes in the ν_{RuH} region and ^1H NMR spectra showed that ruthenium bonded hydride ligand is the coordination site, the dihydrogen bonded ($\text{RuH}\cdots\text{HOR}$) species being the intermediates of proton transfer and non-classical complex formation (Scheme 3).

Upon the addition of increasing amounts of TFE to the solution of $\text{Cp}^*\text{RuH}(\text{dppe})$ in *n*-hexane, whose low polarity favors hydrogen bond formation but not proton transfer, at room temperature, a gradual increase of the ν_{RuH} band intensity was observed. The ν_{RuH} band integral intensity was 1.3 times higher in the presence of 12 equiv. TFE is relative to free **1**. Such changes are consistent with the hydrogen bonding to the hydride ligand [33] and are caused by the overlap of the $\nu_{\text{RuH}}(\mathbf{1})$ and $\nu_{\text{RuH}}(\mathbf{1a})$ bands, of which the latter has higher intensity. The observation of more distinct changes (separate bands) by temperature lowering in this solvent was precluded by the low compound solubility. However, use of a 2:1 v/v *n*-hexane-dichloromethane mix-

Table 3

Parameters of the hydrogen-bonding between $\text{Cp}^*\text{RuH}(\text{dppe})$ and MFE or TFE in CH_2Cl_2

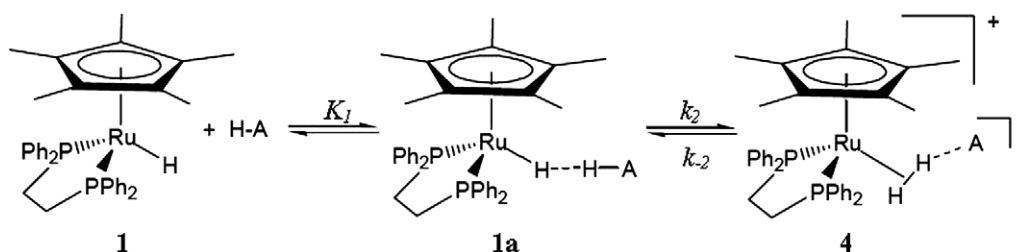
ROH	P_i^a	$\nu_{\text{OH}(\text{free})}$ (cm^{-1})	$\nu_{\text{OH}(\text{bonded})}$ (cm^{-1})	$\Delta\nu$ (cm^{-1})	$\Delta H^{\circ b}$ (cm^{-1})	$\Delta H^{\circ c}$ (cm^{-1})	$\Delta S^{\circ c}$ (eu)	E_j^d
MFE	0.74	3600	3346	254	−4.7	−4.5	−15.8	1.38
TFE	0.89	3590	3254	336	−5.7	−5.7	−23.8	1.39

^a Acidity factors of proton donors [32].

^b Calculated by Eq. (3), mean error $\pm 0.4\text{ kcal mol}^{-1}$.

^c Calculated from the temperature dependence of H-bond formation constants.

^d Basicity factor as defined in Eq. (4), $\Delta H_{11}^\circ = -4.6\text{ kcal mol}^{-1}$ for CH_2Cl_2 [30,31].



Scheme 3.

ture allowed to cool down to 250 K. No growth of the dihydride ν_{RuH} band (at 2000 cm^{-1}) was observed under these conditions, showing that the isomerization is slow in comparison to the experiment timescale. In the presence of the increasing amounts of TFE, the decrease of the ν_{RuH} band of free hydride **1** at 1914 cm^{-1} and the growth of a new band at 1900 cm^{-1} ($\Delta\nu_{\text{RuH}} = -14\text{ cm}^{-1}$), belonging to the Ru–H stretching vibration in the dihydrogen-bonded complex ($\nu_{\text{RuH bonded}}$), was observed (Fig. 4).

Use of neat dichloromethane allowed working at lower temperatures (down to 190 K) but the observation of dihydrogen bonded species was complicated by the proton transfer process, which readily occurs in this solvent at low temperatures. Thus, the addition of 2 equiv. of TFE to a CH_2Cl_2 solution of **1** at 200 K causes a slight increase of the ν_{RuH} band intensity due to the dihydrogen bond formation. However, increasing the TFE excess up to 6 equiv. leads to a very small shift of the ν_{RuH} band (by -2 cm^{-1}) due to the increase of the ν_{RuH} (**1a**) contribution into the overall band and to an intensity decrease because of partial proton transfer with formation of the non-classical dihydride, as was confirmed by NMR.

The ^1H NMR spectra show an up-field shift of the hydride resonance of **1** from -14.17 ppm ($J_{\text{HP}} = 35\text{ Hz}$) to -14.28 ppm ($J_{\text{HP}} = 30\text{ Hz}$) in the presence of up to 2 equiv. TFE in CD_2Cl_2 . The presence of a minor (1%) amount of $[\text{Cp}^*\text{Ru}(\eta^2\text{-H}_2)(\text{dppe})]^+$ (**4**) was shown by the appearance of a signal at -9.49 ppm having a short T_1 relaxation time (ca 30 ms). In the presence of 14 equiv. of TFE, the hydride resonance of **1** shifted further to a stronger field ($\delta_{\text{Ru-H}} = -14.32\text{ ppm}$, $J_{\text{HP}} = 30\text{ Hz}$) (Fig. 5) and the amount of non-classical complex present in the system increased (14%). The signal of **4** disappeared when the temperature increased above 230 K but reappeared upon cooling back, evidencing the reversibility of the proton transfer step (Scheme 3). Such substantial high-field shift of the hydride ligand is in agreement with the formation of the $\text{RuH}\cdots\text{HA}$ hydrogen bond [2].

Further confirmation of $\text{H}\cdots\text{H}$ bond formation was obtained by the measurement of the longitudinal relaxation time (T_1^{obs}) of the hydride signal of **1** in the presence of TFE. As expected, the $T_{1\text{min}}^{\text{obs}}$ value decreases upon addition of the proton donor [2,34]. This decrease is proportional to the amount of alcohol added (Fig. 6), since the corresponding hydride resonance belongs to the mixture of free and hydrogen bonded hydride species and since the hydrogen bonding equilibrium shifts to the right with the increase of alcohol excess. It is also of significance that the temperature corresponding to the $T_{1\text{min}}$ increases slightly upon H-bond formation from 230 to 240 K. This phenomenon signals a decreased correlation time (τ_C), i.e. a slower tumbling motion, for the protonated species, in agreement with its expected larger size. Thus, slightly higher temperatures

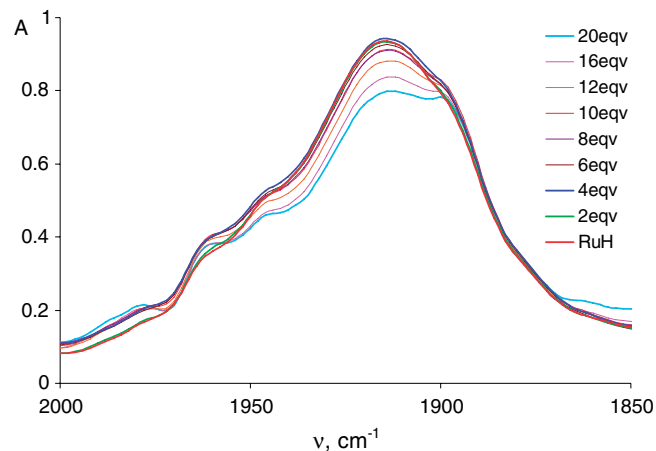


Fig. 4. IR spectra (ν_{RuH} region) of $\text{Cp}^*\text{RuH}(\text{dppe})$ (0.017 M) in the presence of the increasing amounts of TFE. *N*-hexane–dichloromethane 2:1 v/v mixture, 250 K.

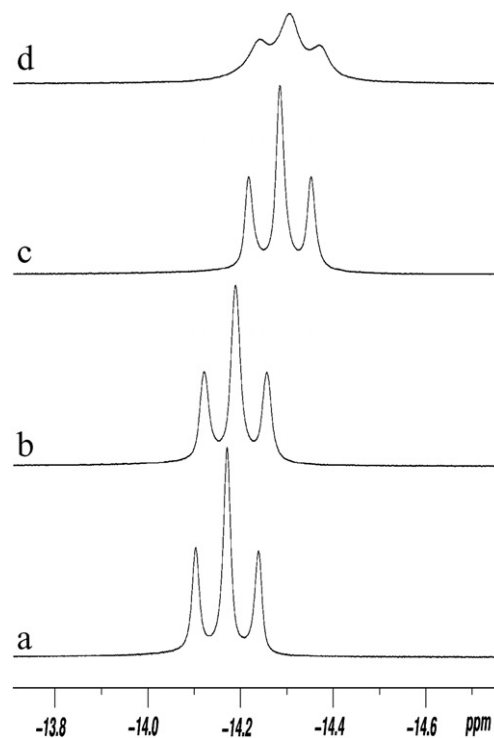


Fig. 5. ^1H NMR spectra (hydride region, CD_2Cl_2 , 200 K) of $\text{Cp}^*\text{RuH}(\text{dppe})$ (a) and $\text{Cp}^*\text{RuH}(\text{dppe})$ in the presence of the increasing amounts of TFE: 0.5 equiv. (b), 2 equiv. (c), 14 equiv. (d).

are needed to raise again τ_C to the conditions required for the most efficient longitudinal relaxation ($w_0^2\tau_C^2 \approx 1$).

No non-classical protonation product was present in the solution at 240 K in the presence of 2 equiv. TFE. Therefore, using the H-bond formation constant value obtained by IR (0.96 M^{-1} at 240 K), it is possible to calculate the amount of $\text{RuH}\cdots\text{HOR}$ species ($x = [\text{RuH}\cdots\text{HOR}]/[\text{RuH}] = 0.11$ at 2-fold TFE excess) and then the value of $T_{1\text{min}}^{\text{obs}}(\text{RuH}\cdots\text{HOR}) = 88\text{ ms}$ for the dihydrogen bonded complex (Eq. (5)).

¹ The partial proton transfer and formation of the non-classical cationic hydride may contribute to the intensity loss at 1914 cm^{-1} .

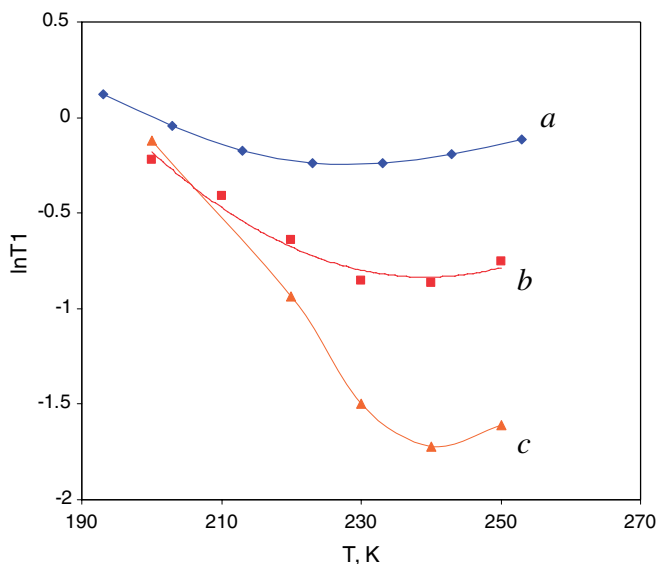


Fig. 6. Temperature dependence of longitudinal relaxation time ($\ln T_1$) for the hydride signal of $\text{Cp}^*\text{RuH}(\text{dhpe})$ (a) in the presence of TFE (2 equiv. – b, 14 equiv. – c) in CD_2Cl_2 solution.

$$1/T_{1\text{min}}^{\text{obs}} = x*1/T_{1\text{min}}^{\text{obs}}(\text{RuH}\cdots\text{HOR}) + (1-x)*1/T_{1\text{min}}(\text{RuH}), \quad (5)$$

$$1/T_{1\text{min}}^{\text{obs}}(\text{RuH}\cdots\text{HOR}) = 1/T_{1\text{min}}(\text{RuH}) + 1/T_{1\text{min}}(\text{H}\cdots\text{H}). \quad (6)$$

In turn, Eq. (6) results in a $T_{1\text{min}}(\text{H}\cdots\text{H})$ time of 100 ms for the hydride–proton dipole–dipole interaction. Application of Eq. (2) to this system gives hydride–proton distance in dihydrogen bonded complex $r(\text{H}\cdots\text{H})$ of 1.38 Å. The same $\text{H}\cdots\text{H}$ distance (1.40 Å) was obtained from the relaxation times measured in the presence of 14 equiv. TFE taking into account the amount of cationic complexes **3** (3%) and **4** (18%) present in solution at 240 K.

Theoretical calculations have been carried out at the DFT B3PW91 level for the model $\text{Cp}^*\text{RuH}(\text{dhpe})$ complex and its adducts with TFE in order to study the relative stability of hydrogen bonded complexes at the metal and hydride sites. The optimised geometries of these two complexes are presented in Fig. 7.

The geometrical changes that accompany hydrogen bond formation are similar to those computed previously at the DFT B3LYP level for $\text{CpRuH}(\text{CO})(\text{PH}_3)$ as a model for $\text{CpRuH}(\text{CO})(\text{PCy}_3)$ [37] and for $\text{Cp}^*\text{FeH}(\text{dhpe})$ as a model for $\text{Cp}^*\text{FeH}(\text{dppe})$ [7]. The hydrogen bond formation is reflected in the lengthening of the OH bond distances ($\Delta r(\text{OH}) = 0.019$ and 0.022 Å for the metal and hydride bonded complexes, respectively) from their values in the isolated proton donors. Note that $\Delta r(\text{OH})$ is greater for the hydride site, signalling stronger bonding. The binding of the proton donors at the hydride site also produces a Ru–H bond lengthening by 0.011 Å, whereas the Ru–H bond does not change upon binding at the metal site ($\Delta r(\text{Ru–H}) = -0.001$ Å).

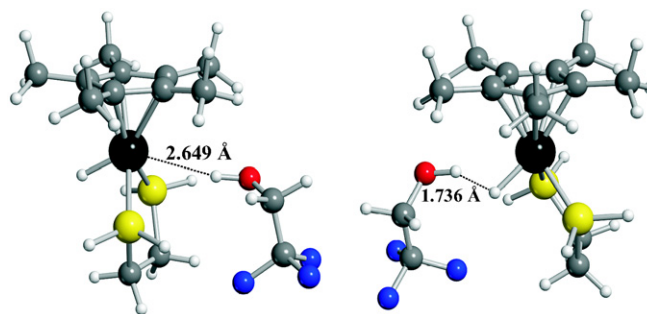


Fig. 7. Optimized geometries of the hydrogen bonded adducts at the hydride and metal sites of model $\text{Cp}^*\text{RuH}(\text{dhpe})$ complex with TFE.

In agreement with such geometrical changes, the energy changes associated with the hydrogen bond formation are more negative for the hydride site than for the metal site, $\Delta E = -10.46$ and -6.72 kcal mol⁻¹, respectively. These values reduce to -5.83 and -1.64 kcal mol⁻¹, respectively, after basis set superposition error (BSSE) correction. Note that the BSSE corrected energy for the hydride bonded adduct is close to the experimentally determined hydrogen bond formation enthalpy (Table 3). Recalculation of the corresponding $\text{Cp}^*\text{FeH}(\text{dhpe})/\text{TFE}$ complexes at the same DFT B3PW91 level of theory gives BSSE corrected hydrogen bond formation energies $\Delta E_{\text{BSSE}} = -0.42$ and -4.92 kcal mol⁻¹ for $\text{Fe}\cdots\text{HOR}$ and $\text{FeH}\cdots\text{HOR}$ complexes, respectively. Thus, the calculations confirm the preference of the proton donor interaction with the hydride ligand and the increase of its basicity going from the iron to ruthenium complex.

Concluding this section, formation of dihydrogen bonded complexes between the ruthenium hydride **1** and alcohols is the first step of the reversible low temperature proton transfer reaction in this system, which precedes the formation of the non-classical cationic hydride complex **4**. In rather low polarity media like dichloromethane (dielectric permittivity ϵ is 14.63 at 200 K [35,36]), ionic species can exist as contact ion pairs additionally stabilized by hydrogen bonding between the η^2 -hydrogens of the cation and the counteranion oxygen atom. The formation of such ion pairs has been shown for some non-classical ruthenium hydrides [4a,37] as well as for the iron analogue $[\text{Cp}^*\text{Fe}(\eta^2\text{-H}_2)(\text{dppe})]^+ \text{X}^-$ [7].

3.4. Interaction with TFA and *p*-nitrophenol – ion pairing in $[\text{Cp}^*\text{Ru}(\eta^2\text{-H}_2)(\text{dppe})]^+ \text{X}^-$

Since the conjugate bases of the fluorinated alcohols used herein are colorless species and do not exhibit any typical IR absorptions that could signal their hydrogen bonding with the product dihydrogen complex, we employed *p*-nitrophenol and trifluoroacetic acid for this study. The UV–Vis and IR bands of these proton donors have been shown to be very sensitive to their protonation and hydrogen bonding status.

In the case of trifluoroacetic acid (TFA), IR spectroscopy can be conveniently used due to sensitivity of the acid

ν_{CO} band and the anion $\nu_{\text{OCO}}^{\text{as}}$ band to hydrogen bonding [7,38,39]. The IR spectra in the carbonyl stretching region were measured at various TFA concentrations (from 0.0075 to 0.075 M) and at different **1**/TFA ratios (from 4:1 to 1:6). Interestingly, no CF_3COO^- anion band was observed in the spectrum for a 2:1 TFA/**1** ratio; two bands at 1734 and 1780 cm^{-1} are assigned to the dihydrogen-bonded complex **1a** and to the acid dimer, respectively. When the temperature was increased up to 240 K, the band at 1734 cm^{-1} decreased reversibly, showing the reversibility of the hydrogen bond formation. Upon increasing the $\text{Cp}^*\text{RuH}(\text{dppe})$ amount, proton transfer occurred and the major band observed under these conditions is at 1687 cm^{-1} (Fig. 8). Note that the bands of the molecular complexes are still present in the spectra at 1:1 TFA/**1** ratio.

Comparison of the spectrum of the 1:1 $\text{Cp}^*\text{RuH}(\text{dppe})/\text{TFA}$ mixture with that of the $\text{CF}_3\text{COO}^- \text{PPh}_4^+$ salt and with that of the $\text{Cp}^*\text{FeH}(\text{dppe})/\text{TFA}$ 1:1 mixture at the same concentration (Fig. 9) shows that the band at 1687 cm^{-1} has high frequency shoulder belonging to the hydrogen bonded ion pair $[\text{Cp}^*(\text{dppe})\text{M}(\eta^2\text{-H}_2)]^+ \cdots [\text{OCOCF}_3]^-$ in the case of iron, but is only slightly asymmetric in the case of ruthenium. Thus, in these rather diluted solutions the major species present is free CF_3COO^- anion, the amount of hydrogen bonded ion pairs being higher in the case of iron than ruthenium.

When using a 6-fold excess of the acid, no bands attributable to the free anion or to the hydrogen-bonded complex are visible, whereas a wide and low intensity band is observed at 1620 cm^{-1} . This corresponds to the free homo-conjugated ion, in which the $[\text{CF}_3\text{COO}]^-$ anion is bonded to two TFA molecules [40].

Evidently, since the trifluoroacetate anion is a weak proton acceptor for hydrogen bonding, it is present in large

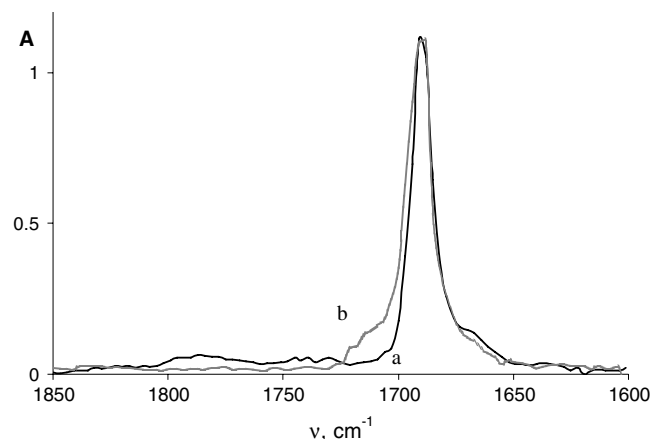


Fig. 9. IR spectra in the $\nu_{\text{CO}}/\nu_{\text{OCO}}^{\text{as}}$ region of TFA (0.075 M) in the presence of equimolar amounts of $\text{Cp}^*\text{RuH}(\text{dppe})$ (a) and $\text{Cp}^*\text{FeH}(\text{dppe})$ (b).

proportions as the free base in solution. In the presence of excess acid, the only carbonyl species present in solution are CF_3COOH and $[\text{CF}_3\text{COO}(\text{HOCCF}_3)_2]^-$.

The equilibrium resulting from the interaction between $\text{Cp}^*\text{RuH}(\text{dppe})$ and a weaker proton donor – *p*-nitrophenol (PNP; $P_i = 1.27$) – was investigated by UV–Vis spectroscopy. Spectra were recorded for CH_2Cl_2 solutions of PNP (0.001 M) in the presence of **1** at different ratios from 1:0.1 to 1:2, in the 200–230 K temperature range, where the observed changes were fully reversible. The spectra show wide overlapping bands of both the phenols in their various forms and the hydride complexes (both free and dihydrogen bonded) (Fig. 10).

The absence of free phenolate is signaled by the absence of a band at 430 nm. A band decomposition yields three bands with maxima at 312, 342, and 384 nm. The first two bands are assigned to free PNP and to the dihydrogen

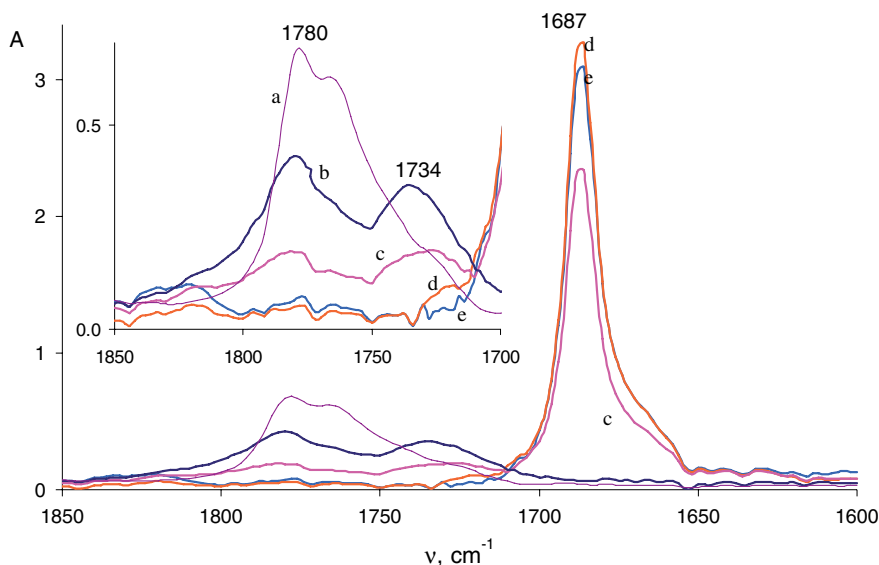


Fig. 8. IR spectra in the $\nu_{\text{CO}}/\nu_{\text{OCO}}^{\text{as}}$ region of TFA (0.0075 M) (a) and TFA in the presence of $\text{Cp}^*\text{RuH}(\text{dppe})$: 0.5 equiv. (b); 1 equiv. (c); 2 equiv. (d); 4 equiv. (e). CH_2Cl_2 , 200 K.

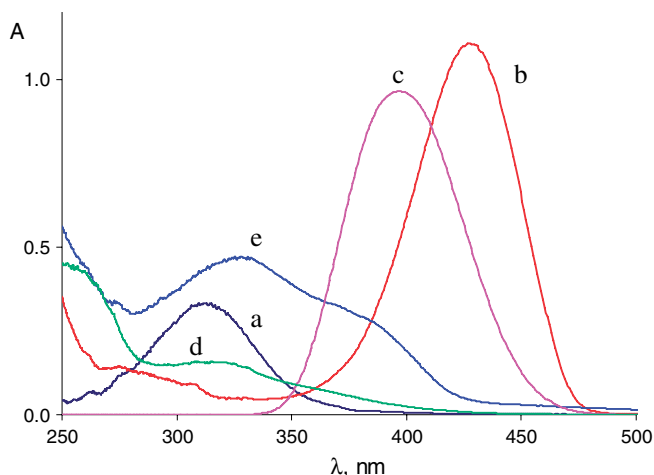


Fig. 10. UV-Vis spectra of PNP (0.001 M) (a), potassium *p*-nitrophenolate (0.001 M in the presence of [18]crown-6) (b), homoconjugated PNP anion (band derived from the spectrum of a 1:1 mixture of (a) and (b)) (c), Cp^{*}RuH(dppe) (0.0005 M) (d) and PNP (0.001 M) in the presence of Cp^{*}RuH(dppe) (0.0005 M) (e). CH₂Cl₂, 200 K.

bonded complex [Cp^{*}(dppe)RuH]·HOC₆H₄NO₂. Note that the 342 nm band is red shifted not only relative to free PNP ($\Delta\lambda = 30$ nm), but also slightly red-shifted with respect to the related iron complex [Cp^{*}(dppe)-FeH]·HOC₆H₄NO₂ (340 nm) [7], in agreement with a slightly stronger hydrogen bonding. The band at 384 nm is attributed to a hydrogen-bonded phenolate ion, since this is blue-shifted from the free phenolate band by 46 nm. The formation of the 1:2 ion pair, stabilized by a hydrogen bond between the non-classical cation and homoconjugated phenolate anion, [Cp^{*}(dppe)M(η^2 -H₂)]⁺·[ArOHOAr]⁻, was shown previously for the iron analogue [7]. The assignment of the absorption at 384 nm to the 1:2 hydrogen-bonded ion pair in the present case was confirmed by the titration experiment. Upon increasing the amount of **1** at constant PNP concentration at 200 K, the bands at 342 nm and 384 nm grow in intensity whereas the free phenol band at 312 nm decreases. The plot of the intensity changes at 380 nm versus the Cp^{*}RuH(dppe) mole fraction (Fig. 11) gives a break point for a mole fraction of (or near) 0.3, indicating a 1:2 binding stoichiometry for the ionic species, [Cp^{*}(dppe)Ru(η^2 -H₂)]⁺[ArOHOAr]⁻. As in the case of iron the 16 nm blue-shift of this band relative to free [ArOHOAr]⁻² suggests further hydrogen bonding of homoconjugated anion with the cationic dihydrogen complex, [Cp^{*}(dppe)Ru(η^2 -H₂)]⁺·[ArOHOAr]⁻. Note that the position of this band is slightly different from that of the iron analogue, in agreement with a higher basicity of **1** and thus a lower acidity of [Cp^{*}(dppe)Ru(η^2 -H₂)]⁺.

² Variable-temperature UV-Vis spectra of the homoconjugated PNP anion were obtained previously by some of us for the equimolar mixture of PNP and potassium *p*-nitrophenolate in the presence of excess [18] crown-6, see Ref. [7].

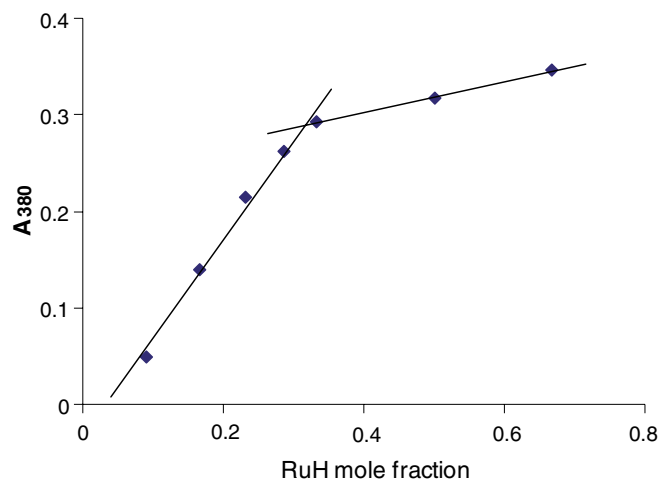


Fig. 11. Intensity changes at 380 nm vs the Cp^{*}RuH(dppe) mole fraction (mole fraction = $C_{\text{RuH}}/(C_{\text{RuH}} + C_{\text{PNP}})$).

The spectral changes are fully reversible in the 200–230 K temperature range, showing that proton transfer is reversible and no significant isomerization to the classical dihydride complex occurs within this temperature range. Upon the temperature decrease, the band of the free phenol decreases and those of hydrogen-bonded phenol (342 nm) and hydrogen bonded ion pair (384 nm) increase. Note that neither the free phenolate band, expected at 420–430 nm, nor the band of homoconjugated anion [ArOHOAr]⁻, expected at ca. 400 nm, were observed, suggesting that the hydrogen bonded ion pair does not essentially dissociate under these conditions.

3.5. Thermodynamics of proton transfer from HFIP

The UV/Vis spectral changes resulting from the interaction between neutral hydride **1** and HBF₄ are shown in Fig. 12. The starting hydride complex has a relatively strong and broad metal–ligand charge-transfer band [41] with a maximum around 320 nm ($\epsilon = 7200$ L mol⁻¹ cm⁻¹

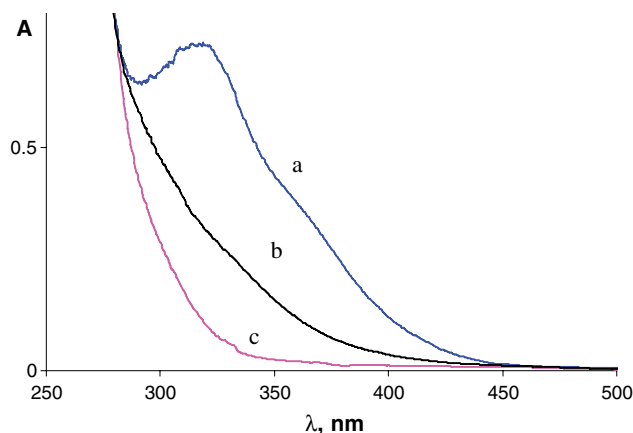


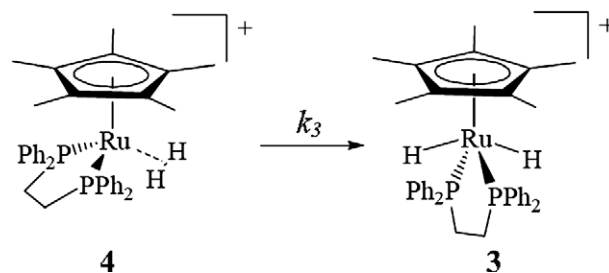
Fig. 12. UV-Vis spectral changes observed for the protonation of Cp^{*}Ru(dppe)H (0.0025 M) by 1 equiv. HBF₄ in CH₂Cl₂. Before addition of HBF₄ ($T = 200$ K) (a); after addition of HBF₄ at 200 K (b) and 290 K (c).

at 200 K, CH_2Cl_2), spectrum a. The dihydrogen complex and the classical hydride, spectra b and c, correspondingly, have much weaker and featureless absorptions (at 320 nm $\epsilon = 3100$ and $970 \text{ L mol}^{-1} \text{ cm}^{-1}$, correspondingly, at 200 K in CH_2Cl_2).

Proton transfer from HFIP was studied by UV–Vis spectroscopy, which proved itself to be very useful for the quantitative measurements. The interaction of $\text{Cp}^*\text{RuH}(\text{dppe})$ with 5 equiv. HFIP in dichloromethane at low temperatures (200–205 K) produces dihydrogen complex **4** (as was confirmed by ^1H NMR spectroscopy) immediately and near quantitatively, which transforms back to the starting hydride complex upon temperature increase, see Fig. 13. The spectrum obtained upon cooling back from 235 to 205 K, is identical to the original one at the same temperature. These UV–Vis spectral changes indicate, in agreement with the IR and NMR data, absence of the isomerization and the reversibility of the proton transfer equilibrium (Scheme 3) within 200–235 K temperature range. These enabled us to obtain the equilibrium constant K_2 for the proton transfer step assuming that all hydride **1** is in the dihydrogen-bonded form **1a** and that the equilibrium involves a second alcohol molecule. The van't Hoff plot (Fig. 13) gives the enthalpy ($\Delta H^\circ = -8.1 \pm 0.6 \text{ kcal mol}^{-1}$) and the entropy ($\Delta S^\circ = -17 \pm 3 \text{ eu}$) of the proton transfer step.

3.6. Isomerization of $[\text{Cp}^*\text{Ru}(\eta^2\text{-H}_2)(\text{dppe})]^+$ into $[\text{Cp}^*\text{Ru}(\text{H})_2(\text{dppe})]^+$

In the presence of more than 2 equiv. of TFE, the proton transfer occurs at 200 K in dichloromethane and subsequent isomerization of non-classical complex **3** into the classical one **4** becomes evident above 240 K (Scheme 4). Interestingly, the $T_{1\text{min}}$ of the dihydride signal of **3** obtained under these conditions increases in comparison



Scheme 4.

with the BF_4^- salt (Table 1), being 599 ms at 220 K. A possible interpretation of this difference is a stronger hydrogen bonding between one or two hydride ligands of **3** with the stronger conjugate base $\text{CF}_3\text{CH}_2\text{O}^-$, thereby increasing the average $\text{H} \cdots \text{H}$ distances.

However, TFE gives only partial proton transfer even at quite high concentrations (up to 20 equiv.), therefore, as was shown for the iron analogue [7,8], the accurate determination of the rate constant for the isomerization of $[\text{Cp}^*\text{Ru}(\eta^2\text{-H}_2)(\text{dppe})]^+$ (**4**) obtained with these alcohols at different temperatures would be thwarted by coupling between two key rate constants – k_3 (Scheme 4) and k_{-2} (Scheme 3) leading from the dihydrogen complex back to the starting monohydride. The isomerization rate constant $k_{3\text{obs}}$ for HFIP at 250 K (2.5 equiv. HFIP give ca. 40% of **4**) was estimated as $3 \times 10^{-4} \text{ s}^{-1}$. The use of $\text{HBF}_4 \cdot \text{Et}_2\text{O}$ allowed studying the process in Scheme 4 under clean first order conditions. Thus, the dihydrogen complex **4** was generated quantitatively in situ by low temperature (195 K) addition of the acid (58% $\text{HBF}_4 \cdot \text{Et}_2\text{O}$) to the solution of **1** in dichloromethane. The isomerization reaction (Scheme 4) could be studied by IR measurements of the increase of the dihydride complex **3** ν_{RuH} band at 2000 cm^{-1} (representative set of spectral changes is shown in Fig. 2). However,

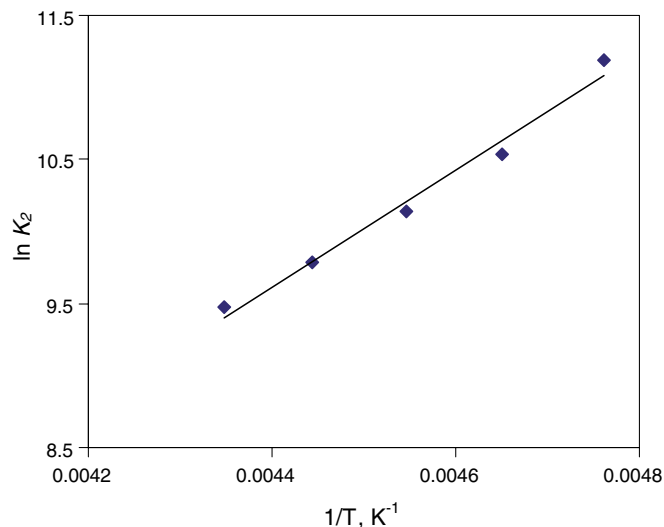
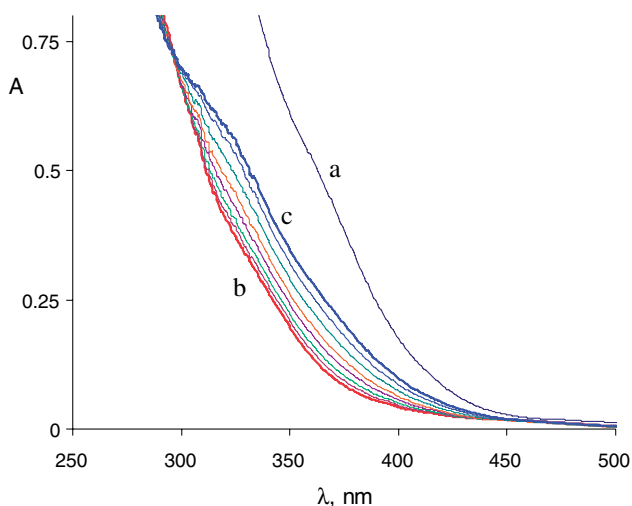


Fig. 13. UV–Vis spectra of $\text{Cp}^*\text{RuH}(\text{dppe})$ (0.0035 M) in the presence of 5 equiv. HFIP in CH_2Cl_2 (left) and the corresponding dependence of $\ln K_2$ vs temperature (right). Free hydride at 200 K (a); in the presence of HFIP at 205 K (b) and 235 K (c). The intermediate spectra correspond to 230–205 K (5 K steps).

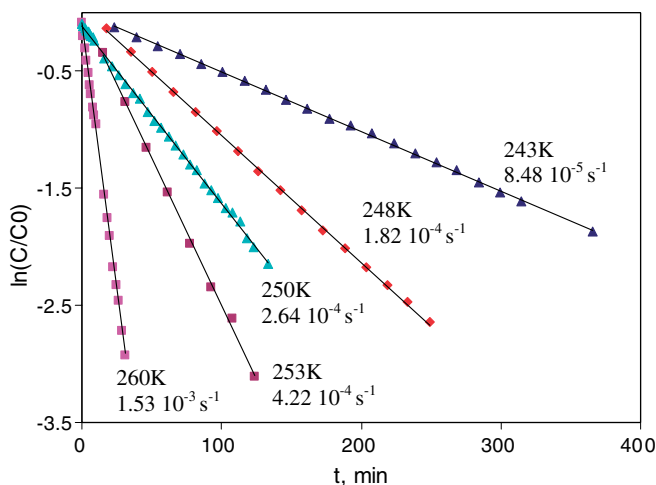


Fig. 14. Logarithmic plots of the $[\text{Cp}^*\text{Ru}(\eta^2\text{-H}_2)(\text{dppe})]^+\text{BF}_4^-$ resonance decay. Temperatures and the corresponding rate constants are indicated near to the lines.

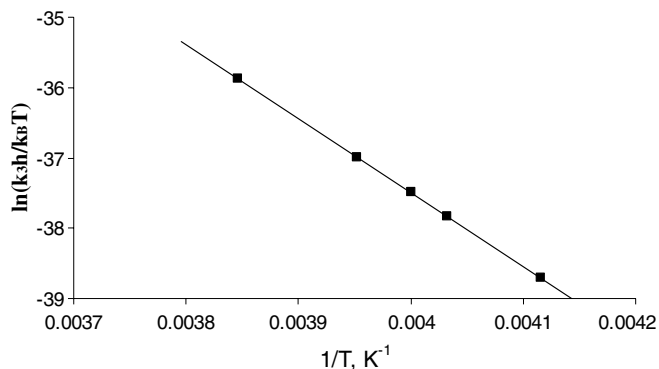


Fig. 15. Eyring plot for the isomerization rate constant k_3 .

as in the case of the iron analogue [8], the NMR monitoring of the process was much more convenient, providing the concentrations of both non-classical (4) and classical (3) species as well as directly probing for the formation of possible decomposition products during the measurements.³ Both the decay of the dihydrogen complex resonance and the growth of the dihydride complex resonance were monitored by ^1H NMR spectroscopy. The non-classical resonance decay gives an excellent fit to the first order rate law at each temperature (Fig. 14), yielding the rate constants k_3 reported in Fig. 14. The Eyring analysis of the rate constants k_3 (Fig. 15) yields the activation parameters $\Delta H^\ddagger = 20.9 \pm 0.8 \text{ kcal mol}^{-1}$ and $\Delta S^\ddagger = 9 \pm 3 \text{ eu}$. The activation enthalpy and entropy values are close to those found for the iron analogue ($\Delta H^\ddagger = 21.6 \pm 0.8 \text{ kcal mol}^{-1}$, $\Delta S^\ddagger = 5 \pm 3 \text{ eu}$ [8]) and similar to those previously reported for related ruthenium derivatives [24d,42].

4. Discussion

4.1. Proton accepting properties of the hydride ligand

As pointed out in Section 1, the data on the metal influence on the hydrogen bonding site nature and the proton accepting properties of the hydride ligand are still scarce. Herein, we have found that the first step of the $\text{Cp}^*\text{RuH}(\text{dppe})$ interaction with proton donors is the dihydrogen bond formation. The preference of the proton donor coordination to the hydride ligand is confirmed by theoretical calculations. The basicity factor E_j of the ruthenium bound hydride ligand (1.39) is only slightly higher than that of the $\text{Cp}^*\text{FeH}(\text{dppe})$ ($E_j = 1.35$ [6]). This is quite surprising, since a much more pronounced basicity increase down the Group was found for the series of PP_3MH_2 hydrides ($\text{PP}_3 = \kappa^4\text{-P}(\text{CH}_2\text{CH}_2\text{PPh}_2)_3$), E_j values being equal to 1.12 for $\text{M} = \text{Fe}$ and 1.33 for $\text{M} = \text{Ru}$ [4b]. The possible explanation for this phenomenon could be in the steric influence of the ancillary ligands, which apparently impose high steric constraints in the case of $\text{Cp}^*\text{RuH}(\text{dppe})$. This is evident from the high hydrogen bond entropy value $\Delta S^\circ = -23.8 \text{ eu}$ for $\text{Cp}^*\text{RuH}(\text{dppe})/\text{TFE}$ complex, which is almost twice higher than that for $\text{Cp}^*\text{FeH}(\text{dppe})/\text{TFE}$ (-13.6 eu), whereas the enthalpy values differ by only $0.3 \text{ kcal mol}^{-1}$ ($\Delta H^\circ = -5.7$ and $-5.4 \text{ kcal mol}^{-1}$ for RuH and FeH , respectively).

4.2. Proton transfer mechanism

Despite the steric encumbrances to hydrogen bond formation, proton transfer easily occurs in this system yielding the cationic non-classical $[\text{Cp}^*\text{Ru}(\eta^2\text{-H}_2)(\text{dppe})]^+\text{A}^-$ complex, whose formation is shown here for the first time. The proton transfer from TFE, HFIP and PNP is not quantitative under the proton donor excesses used and is reversible within the temperature range 190–230 K, the equilibrium (Scheme 3) shifting to the right with temperature decrease. This signals a proton transfer exothermicity. In low polarity media like dichloromethane, ionic species should exist as contact ion pairs [43], which could additionally be stabilized by hydrogen bonding between the cation and anion. There is also a question about the anion composition, which could be additionally bonded to its conjugated acid, forming the so-called homoconjugate anion $[\text{AHA}]^-$. In the case of the quite strong acid TFA, the $[\text{AHA}]^-$ formation occurs in the presence of high acid excess. The major species in solution is the free CF_3COO^- anion, the amount of hydrogen bonded ion pairs being higher in the case of iron than ruthenium. However, for the weaker proton donor *p*-nitrophenol, formation of the hydrogen bonded ion pair $[\text{Cp}^*(\text{dppe})\text{Ru}(\eta^2\text{-H}_2)]^+\cdots[\text{ArOHOAr}]^-$ was confirmed by means of UV–Vis spectroscopy. Thus, one can argue that for even weaker proton donors such as TFE and HFIP, having stronger conjugated bases, the non-classical complex does exist as the contact ion pair additionally stabilized by hydrogen bonding between the cation and the

³ The sum of the integrals, after normalization relative to the solvent peak used as an internal standard, was relatively constant throughout the reaction, showing almost no decomposition.

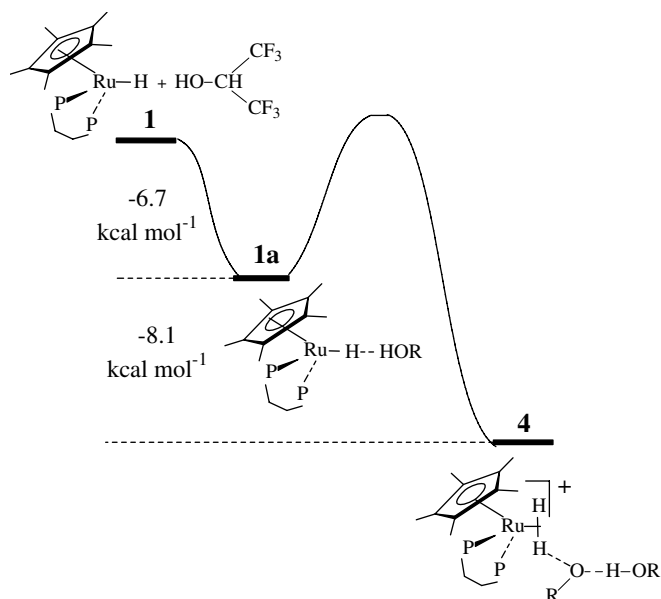


Fig. 16. Energy (ΔH°) profile for protonation of $\text{Cp}^*\text{RuH}(\text{dppe})$ by HFIP.

homoconjugate anion. Involvement of the second alcohol molecule in the proton transfer to the hydride ligand strengthens the primary hydrogen bond, making the activation barrier lower, and stabilizes the proton transfer product through the formation of the hydrogen bonded ion pair with the homoconjugate anion as was shown both experimentally and theoretically for $\text{Cp}^*\text{FeH}(\text{dppe})$ [6,7]. The dihydrogen-bonding and $[\text{Cp}^*\text{Ru}(\eta^2\text{-H}_2)(\text{dppe})]^+$ formation are immediate in the time-scale of the conventional spectroscopies used. The equilibrium between these two species shifts toward the dihydrogen complex when stronger proton donors, higher alcohol/hydride ratios, or lower temperatures are employed. Assuming the same scheme, the thermodynamic parameters (ΔH° and ΔS°) of proton transfer from HFIP to $\text{Cp}^*\text{RuH}(\text{dppe})$ were calculated, which appeared to be more negative than those for the $\text{Cp}^*\text{FeH}(\text{dppe})$ / HFIP system [7]. The hydrogen bond formation enthalpy for this alcohol was obtained using Eq. (2) ($\Delta H^\circ = -6.7 \text{ kcal mol}^{-1}$) and thus the two-well energy profile (Fig. 16) can be drawn for this system. The energy of the transition state leading to complex **4** is drawn qualitatively only. The free activation energy (12–16 kcal mol^{-1}) can be estimated on the basis of the NMR (lack of line broadening) and IR (lack of spectral evolution at the temperatures used) results [2]. This is the first time that a comparison can be made between two metals from the same Group in terms of the enthalpy profile of a proton transfer reaction. The data obtained show that both hydrogen bonding and proton transfer enthalpy increase down the Group.

5. Conclusions

The combined experimental and theoretical study of the interaction between $\text{Cp}^*\text{RuH}(\text{dppe})$ and proton donors of different strengths showed that general features of this pro-

cess are similar to those established for the iron analogue, $\text{Cp}^*\text{FeH}(\text{dppe})$, as well as other transition metal hydride complexes. In the course of this study, the formation of the previously unknown non-classical complex, $[\text{Cp}^*\text{Ru}(\eta^2\text{-H}_2)(\text{dppe})]^+$, was observed at low temperatures, and was preceded by the dihydrogen bonding step. The thermodynamic parameters for dihydrogen bond formation and proton transfer are found to increase on descending the Group from iron to ruthenium, whereas the activation parameters for the subsequent $[\text{Cp}^*\text{M}(\eta^2\text{-H}_2)(\text{dppe})]^+ \rightarrow \text{trans-}[\text{Cp}^*\text{M}(\text{H})_2(\text{dppe})]^+$ isomerization are very similar. Such a comparison has been made for the first time and will be extended to the osmium analogue in our future work.

Acknowledgments

The authors are very grateful to Profs. L.M. Epstein, E.S. Shubina, R. Poli and A. Lledos, friends and tutors, for their support of our research activities and for the help in preparation of this manuscript. Thanks are expressed to Dr. Y. Coppel (LCC, Toulouse) for the assistance in low temperature NMR experiments. This work was supported by the European Commission through the HYDROCHEM program (contract HPRN-CT-2002-00176), a bilateral PICS Grant (France–Russia), RFBR Grants (05-03-22001, 05-03-32415) and the Division of Chemistry and Material Sciences of RAS (Russia). M.B. thanks the Spanish Ministerio de Educación y Ciencia for a post-doctoral fellowship.

References

- [1] M. Peruzzini, R. Poli (Eds.), Recent Advances in Hydride Chemistry, Elsevier, Amsterdam, 2001.
- [2] N.V. Belkova, E.S. Shubina, L.M. Epstein, Acc. Chem. Res. 38 (2005) 624.
- [3] (a) D.M. Heinekey, W.J. Oldham, Chem. Rev. 93 (1993) 913; (b) G.J. Kubas, Metal Dihydrogen and σ -Bond Complexes, Kluwer Academic/Plenum Press, New York, 2001.
- [4] (a) E.I. Gutsul, N.V. Belkova, G.M. Babakhina, L.M. Epstein, E.S. Shubina, C. Bianchini, M. Peruzzini, F. Zanobini, Russ. Chem. Bull., Int. Ed. 52 (2003) 1204; (b) E.I. Gutsul, N.V. Belkova, M.S. Sverdlov, L.M. Epstein, E.S. Shubina, V.I. Bakhmutov, T.N. Gribanova, R.M. Minyaev, C. Bianchini, M. Peruzzini, F. Zanobini, Chem. Eur. J. 9 (2003) 2219.
- [5] (a) J. Andrieu, N.V. Belkova, M. Besora, E. Collange, L.M. Epstein, A. Lledós, R. Poli, P.O. Revin, E.S. Shubina, E.V. Vorontsov, Russ. Chem. Bull. 52 (2003) 2679; (b) N.V. Belkova, P.O. Revin, M. Besora, M. Baya, L.M. Epstein, A. Lledós, R. Poli, E.S. Shubina, E.V. Vorontsov, Eur. J. Inorg. Chem. (2006) 2192.
- [6] N.V. Belkova, P.O. Revin, L.M. Epstein, E.V. Vorontsov, V.I. Bakhmutov, E.S. Shubina, E. Collange, R. Poli, J. Am. Chem. Soc. 125 (2003) 11106.
- [7] N.V. Belkova, E. Collange, P. Dub, L.M. Epstein, D.A. Lemenovskii, A. Lledós, O. Maresca, F. Maseras, R. Poli, P.O. Revin, E.S. Shubina, E.V. Vorontsov, Chem. Eur. J. 11 (2005) 873.
- [8] M. Baya, O. Maresca, R. Poli, Y. Coppel, F. Maseras, A. Lledós, N.V. Belkova, P.A. Dub, L.M. Epstein, E.S. Shubina, Inorg. Chem. (2006), in press.
- [9] D.-H. Lee, J. Korean Chem. Soc. 36 (1992) 248.
- [10] H. Guan, M. Iimura, M.P. Magee, J.R. Norton, G. Zhu, J. Am. Chem. Soc. 127 (2005) 7805.

- [11] K. Kirchner, K. Mauthner, K. Mereiter, R. Schmid, *J. Chem. Soc., Chem. Commun.* (1993) 892.
- [12] F. Morandini, A. Dondana, I. Munari, G. Pilloni, G. Consiglio, A. Sironi, M. Moret, *Inorg. Chim. Acta* 282 (1998) 163.
- [13] M.J. Frisch, G.W. Trucks, H.B. Schlegel, G.E. Scuseria, M.A. Robb, J.R. Cheeseman, J.A. Montgomery Jr., T. Vreven, K.N. Kudin, J.C. Burant, J.M. Millam, S.S. Iyengar, J. Tomasi, V. Barone, B. Mennucci, M. Cossi, G. Scalmani, N. Rega, G.A. Petersson, H. Nakatsuji, M. Hada, M. Ehara, K. Toyota, R. Fukuda, J. Hasegawa, M. Ishida, T. Nakajima, Y. Honda, O. Kitao, H. Nakai, M. Klene, X. Li, J.E. Knox, H.P. Hratchian, J.B. Cross, V. Bakken, C. Adamo, J. Jaramillo, R. Gomperts, R.E. Stratmann, O. Yazyev, A.J. Austin, R. Cammi, C. Pomelli, J.W. Ochterski, P.Y. Ayala, K. Morokuma, G.A. Voth, P. Salvador, J.J. Dannenberg, V.G. Zakrzewski, S. Dapprich, A.D. Daniels, M.C. Strain, O. Farkas, D.K. Malick, A.D. Rabuck, K. Raghavachari, J.B. Foresman, J.V. Ortiz, Q. Cui, A.G. Baboul, S. Clifford, J. Cioslowski, B.B. Stefanov, G. Liu, A. Liashenko, P. Piskorz, I. Komaromi, R.L. Martin, D.J. Fox, T. Keith, M.A. Al-Laham, C.Y. Peng, A. Nanayakkara, M. Challacombe, P.M.W. Gill, B. Johnson, W. Chen, M.W. Wong, C. Gonzalez, J.A. Pople, GAUSSIAN 03, Revision C.02, Gaussian, Inc., Wallingford, CT, 2004.
- [14] (a) A.D. Becke, *J. Chem. Phys.* 98 (1993) 5648;
(b) J.P. Perdew, in: P. Ziesche, H. Eschrig (Eds.), *Electronic Structure of Solids*, vol. 91, Akademie Verlag, Berlin, 1991, p. 11;
(c) J.P. Perdew, Y. Wang, *Phys. Rev. B* 45 (1992) 13244.
- [15] (a) W.R. Wadt, P.J. Hay, *J. Chem. Phys.* 82 (1985) 284;
(b) P.J. Hay, W.R. Wadt, *J. Chem. Phys.* 82 (1985) 299.
- [16] A. Höllwarth, M. Bohme, S. Dapprich, A. Ehlers, A. Gobbi, V. Jonas, K. Kohler, R. Stegmann, A. Veldkamp, G. Frenking, *Chem. Phys. Lett.* 208 (1993) 237.
- [17] (a) R. Ditchfield, W.J. Hehre, J.A. Pople, *J. Chem. Phys.* 54 (1971) 724;
(b) W.J. Hehre, R. Ditchfield, J.A. Pople, *J. Chem. Phys.* 56 (1972) 2257;
(c) P.C. Hariharan, J.A. Pople, *Mol. Phys.* 27 (1974) 209;
(d) M.S. Gordon, *Chem. Phys. Lett.* 76 (1980) 163;
(e) P.C. Hariharan, J.A. Pople, *Theo. Chim. Acta* 28 (1973) 213;
(f) J.-P. Blaudeau, M.P. McGrath, L.A. Curtiss, L. Radom, *J. Chem. Phys.* 107 (1997) 5016;
(g) M.M. Francl, W.J. Pietro, W.J. Hehre, J.S. Binkley, D.J. DeFrees, J.A. Pople, M.S. Gordon, *J. Chem. Phys.* 77 (1982) 3654;
(h) R.C. Binning Jr., L.A. Curtiss, *J. Comput. Chem.* 11 (1990) 1206;
(i) V.A. Rassolov, J.A. Pople, M.A. Ratner, T.L. Windus, *J. Chem. Phys.* 109 (1998) 1223;
(j) V.A. Rassolov, M.A. Ratner, J.A. Pople, P.C. Redfern, L.A. Curtiss, *J. Comput. Chem.* 22 (2001) 976.
- [18] S.F. Boys, F. Bernardi, *Mol. Phys.* 19 (1970) 553.
- [19] (a) M.I. Bruce, M.G. Humphrey, A.G. Swincer, R.C. Wallis, *Aust. J. Chem.* 37 (1984) 1747;
(b) H. Guan, M. Iimura, M.P. Magee, J.R. Norton, K.E. Janak, *Organometallics* 22 (2003) 4084.
- [20] K.-T. Smith, C. Rømming, M. Tilset, *J. Am. Chem. Soc.* 115 (1993) 8681.
- [21] C. Rømming, K.-T. Smith, M. Tilset, *Inorg. Chim. Acta* 259 (1997) 281.
- [22] R. Poli, M. Baya, R. Meunier-Prest, S. Raveau, *New J. Chem.* 30 (2006) 759.
- [23] O.B. Ryan, M. Tilset, V.D. Parker, *J. Am. Chem. Soc.* 112 (1990) 2618.
- [24] (a) G. Jia, C.-P. Lau, *Coord. Chem. Rev.* 190–192 (1999) 83;
(b) G. Jia, R.H. Morris, *J. Am. Chem. Soc.* 113 (1991) 875;
(c) G. Jia, A.J. Lough, R.H. Morris, *Organometallics* 11 (1992) 161;
(d) M.S. Chinn, D.M. Heinekey, *J. Am. Chem. Soc.* 112 (1990) 5166.
- [25] G. Jia, W.S. Ng, H.S. Chu, W.-T. Wong, N.-T. Yu, I.D. Williams, *Organometallics* 18 (1999) 3597.
- [26] P.A. Maltby, M. Schlaf, M. Steinbeck, A.J. Lough, R.H. Morris, W.T. Klooster, T.F. Koetzle, R.C. Srivastava, *J. Am. Chem. Soc.* 118 (1996) 5396.
- [27] (a) K.A. Earl, G. Jia, P.A. Maltby, R.H. Morris, *J. Am. Chem. Soc.* 113 (1991) 3027;
(b) P.J. Desrosiers, L. Cai, Z. Lin, R. Richards, J. Halpern, *J. Am. Chem. Soc.* 113 (1991) 4173.
- [28] (a) L.M. Epstein, N.V. Belkova, E.I. Gutsul, E.S. Shubina, *Polish J. Chem.* 77 (2003) 1371;
(b) E.S. Shubina, A.N. Krylov, N.V. Belkova, L.M. Epstein, A.P. Borisov, V.D. Mahaev, *J. Organomet. Chem.* 493 (1995) 275;
(c) R.B. Girling, P. Grebenik, R.N. Perutz, *Inorg. Chem.* 25 (1986) 31;
(d) K. Abdur-Rashid, T.P. Fong, B. Greaves, D.G. Gusev, J.G. Hinman, S.E. Landau, A.J. Lough, R.H. Morris, *J. Am. Chem. Soc.* 122 (2000) 9155.
- [29] L.M. Epstein, N.V. Belkova, E.S. Shubina, in: M. Peruzzini, R. Poli (Eds.), *Recent Advances in Hydride Chemistry*, Elsevier, Amsterdam, 2001, p. 391.
- [30] A.V. Iogansen, *Spectrochim. Acta A* 55 (1999) 1585.
- [31] A.V. Iogansen, *Theor. Exp. Khim.* 7 (1971) 312.
- [32] A.V. Iogansen, *Theor. Exp. Khim.* 7 (1971) 302.
- [33] N.V. Belkova, E.S. Shubina, E.I. Gutsul, L.M. Epstein, I.L. Eremenko, S.E. Nefedov, *J. Organomet. Chem.* 610 (2000) 58.
- [34] V.I. Bakhmutov, *Eur. J. Inorg. Chem.* (2005) 245.
- [35] S.O. Morgan, H.H. Lowry, *J. Phys. Chem.* 34 (1930) 2385.
- [36] S. Sharif, G.S. Denisov, M.D. Toney, H.-H. Limbach, *J. Am. Chem. Soc.* 128 (2006) 3375.
- [37] N.V. Belkova, M. Besora, L.M. Epstein, A. Lledós, F. Maseras, E.S. Shubina, *J. Am. Chem. Soc.* 125 (2003) 7715.
- [38] N.V. Belkova, A.V. Ionidis, L.M. Epstein, E.S. Shubina, S. Gruendemann, N.S. Golubev, H.-H. Limbach, *Eur. J. Inorg. Chem.* (2001) 1753.
- [39] E.S. Shubina, N.V. Belkova, L.M. Epstein, *J. Organomet. Chem.* 536–537 (1997) 17.
- [40] J.Z. Dega-Szafran, M. Grundwald-Wyspianska, M. Szafran, *Spectrochim. Acta A* 47 (1991) 543.
- [41] A.B.P. Lever, *Inorganic Electronic Spectroscopy*, second ed., Elsevier, Amsterdam, 1984.
- [42] I. de Los Ríos, M. Jiménez-Tenorio, J. Padilla, M.C. Puerta, P. Valerga, *Organometallics* 15 (1996) 4565.
- [43] A. Macchioni, *Chem. Rev.* 105 (2005) 2039.